 CMC, vol.24, no.1, pp.43-60, 2011

Dynamic Failure Behavior of Nanocrystalline Cu at Atomic Scales

A. M. Dongare[1,2], **A. M. Rajendran**[3], **B. LaMattina**[4], **M. A. Zikry**[1]
D. W. Brenner[1]

Abstract: Large-scale molecular dynamics (MD) simulations are used to investigate the effects of microstructure and loading conditions on the dynamic failure behavior of nanocrystalline Cu. The nucleation, growth, and coalescence of voids is investigated for the nanocrystalline metal with average grain sizes ranging from 6 nm to 12 nm (inverse Hall-Petch regime) for conditions of uniaxial expansion at constant strain rates ranging from $4x10^7$ s^{-1} to 10^{10} s^{-1}. MD simulations suggest that the evolution of voids can be described in two stages: The first stage corresponds to the nucleation of voids and the fast linear initial growth of all the individual voids. The second stage of void growth corresponds to the steady (slower) growth and coalescence of the void aggregates/clusters. The evolution of void fraction is found to be strongly dependent on the loading strain rates, but is less dependent on the grain size of the nanocrystalline metal. Higher strain rates require larger plastic strains to nucleate voids, whereas the larger grain sizes require lower plastic strains to nucleate voids in the inverse Hall-Petch regime. The spall strength of the nanocrystalline metal is less affected by the grain size, but is strongly affected by the loading strain rates.

Keywords: Nanocrystalline metals; Spallation; Molecular dynamics; Voids, Dynamic failure.

1 Introduction

Dynamic fracture (spallation) of ductile metals is attributed to the nucleation of voids that grow and coalesce to form a fracture surface [Knott 1973]. The spall behavior of materials is typically studied using plate impact experiments [Curran,

[1] North Carolina State University, Raleigh, NC, U.S.A.
[2] Author to whom correspondence should be addressed, E-mail: amdongare@ncsu.edu
[3] University of Mississippi, University, MS, U.S.A
[4] US Army Research Office, Research Triangle Park, NC, U.S.A

Seaman and Shockey 1987] wherein a flyer-plate is impacted on to a target plate at a very high velocity. The impact generates compressive waves in the projectile and the target plates that reach the opposite surface and reflect as tensile waves. The reflected tensile waves interact with each other and produce a triaxial stress state under conditions of uniaxial tensile strain. Multiple voids are observed to nucleate in this region experiencing the triaxial tensile stress (defined as the spall plane). The voids grow and coalesce to form microscopic cracks and failure results in a slab of detached material being ejected from the back surface of the material. Plate impact experiments typically result in peak strain rates of 10^5 s^{-1} - 10^6 s^{-1} [Curran, Seaman and Shockey 1987, Minich et al. 2004; Rivas et al. 2000; Fowler et al. 2000], whereas, use of laser-shocks results in peak strain rates of 10^7 s^{-1} - 10^8 s^{-1} [Tamura et al. 2001; Moshe et al. 1999 and 1998; Kanel et al. 1993; Eliezer, Gilath, and Bar-Noy 1990Meyers 1994]. Research over the past decades has focused on developing the ability to understand and predict the failure response of materials under dynamic loading conditions. Soft-recovery experiments suggested that the voids in ductile materials are generally observed to be almost spherical that nucleate at grain boundaries due to GB sliding and/or dislocation pileups during impact loading [Curran, Seaman and Shockey 1987]. Most of the spall experiments, however, are aimed at evaluating the spall strength (peak tensile pressure prior to failure) of the material and the understanding of the effects of microstructure and loading conditions on the nucleation, growth, and coalescence of voids at the onset of spall failure is still in its infancy. The lack of understanding can be attributed to the small time scales of these processes which make it difficult to identify and characterize these processes using experiments alone.

The capabilities of current computer simulations allow the modeling of these phenomena and can therefore complement experiments in the characterization of the micromechanisms related to deformation and failure at high strain rates. Most of the modeling of failure of ductile metals has been carried out using continuum models that use Gurson-type models [Gurson 1977; Tvergaard and Needleman 1984] to address the mechanism of void growth and porosity. These models, however, predict void growth under quasi-static loading conditions and are found to be inapplicable to model void growth behavior at high strain rates [Dongare et al. 2009a]. A few models of spall-failure [Thomason 1999; Rajendran, Dietenberger, and Grove 1989; Wright and Ramesh 2008] have been developed to describe the void-growth based failure in metals during plate impact experiments. Although the void growth process is modeled explicitly in these simulations, approximations are made to account for nucleation, growth, and coalescence of the voids and for the dependence of strain rate and microstructure on these processes. These micro-mechanisms related to ductile failure under dynamic loading conditions can be investigated by

using molecular dynamics (MD) simulations, which can provide the atomic level detail needed for the physical understanding and interpretation of experimental observations at high strain rates. MD simulations have been employed to study the micro-mechanisms associated with void growth in single-crystal systems [Seppala, Belak and Rudd 2004; Dongare et al. 2008; Traiviratana et al. 2008], and coalescence [Seppala, Belak and Rudd 2004 and 2005] for loading conditions at the spall plane at strain rates $\geq 10^8$ s^{-1}. The initial system in these studies, however, is a clean (damage/defect free) single crystal system with a pre-existing void equilibrated to zero pressure. Thus, the micro-mechanisms related to nucleation of voids are neglected in these simulations. The MD simulations of deformation suggest that void growth occurs through the heterogeneous nucleation of dislocations from the void surface. In addition, the simulations also suggest that two neighboring voids coalesce through a development of slip planes between the voids.

Recently, these studies have been extended to investigate the micromechanisms related to void nucleation and growth in nanocrystalline Cu [Dongare et al. 2009b] for uniaxial strain tensile deformation conditions at a constant strain rate of 10^8 s^{-1} and under conditions of shock loading induced spall [Dongare et al. 20010a]. These simulations suggest that the presence of a large volume fraction of grain boundaries in the nanocrystalline system has an effect on the micromechanisms of dynamic failure. Voids are observed to nucleate at a triple junction of grain boundaries and grow along the boundaries. The nucleation of the void is attributed to mechanical separation/sliding at triple point junctions in contrast to dislocation pile-ups observed in polycrystalline metals. The nucleation of the void causes a shell of disordered material surrounding the void and further growth of the void is observed to occur by the shearing of the neighboring disordered material. This mechanism results in a fast initial growth of the void (defined as stage I) that causes an increase in the temperature of the system, which in turn, results in the recrystallization of the disordered material. The recrystallization of the surrounding material results in a slower growth of the void (defined as stage II). The simulations [Dongare et al. 2009b, Dongare et al. 2010a] therefore demonstrate two stages of growth of a void during failure under conditions of uniaxial tensile strain in nanocrystalline Cu at a constant strain rate of 10^8 s^{-1}. The effects, however, are unknown.

The objective of this paper is to understand the effects of microstructure (grain size) and loading conditions (strain rates) of the on the micromechanisms related to failure of nanocrystalline Cu under dynamic loading conditions. The nucleation, growth, and coalescence of voids and the evolution of void fraction is investigated for the nanocrystalline metal with average grain sizes ranging from 6 nm to 12 nm (inverse Hall-Petch regime) for conditions of uniaxial expansion at constant strain rates ranging from $4x10^7$ s^{-1} to 10^{10} s^{-1}. The grain sizes in the inverse Hall-Petch

regime are chosen here due to the ultra-high strengths of the nanocrystalline metal under conditions of shock loading at these grain sizes [Bringa et al. 2005]. The MD simulations, as will be discussed in the later sections, suggest a strong influence of the loading strain rates on the evolution of the void fraction and the subsequent spall strengths of the nanocrystalline metal. The computational details are presented in section 2. The effects of grain size and loading strain rates on the microstructural evolution of the nanocrystalline metal and the stress-strain profiles are discussed in Sections 3 and 4, respectively. The relevance of these results to the modeling of spall behavior at the continuum scale is discussed in Section 5.

2 Computational Details

The MD computational cell used here can be considered as being part of the material belonging to the incipient spall plane that experiences the triaxial tensile stress conditions generated due to the uniaxial strain conditions of loading. Large scale MD simulations using the of the Embedded Atom Method (EAM) potential [Voter 1994] are carried out to study the micromechanisms related to dynamic failure in nanocrystalline Cu subjected to uniaxial tensile strain loading. This EAM potential is well suited to describe deformation behavior for Cu as it provides a good description of the deformation [Dongare et al. 2010b] and failure behavior [Dongare et al. 2009b] of nanocrystalline Cu. The elements of the atomic-level stress tensor were calculated as

$$\sigma_{\alpha\beta}(i) = -\frac{1}{\Omega_0}\left[\frac{1}{2}\sum_j F_{ij}^{\alpha} r_{ij}^{\beta} + M_i v_i^{\alpha} v_i^{\beta}\right] \tag{1}$$

where α and β label the Cartesian components, Ω_0 is the atomic volume, F_{ij} is the force on atom i due to atom j, M_i is the mass of atom i, and v_i is the velocity of atom$i$. While, a recently developed atomic-level stress tensor [Shen and Atluri 2004] proves to be more accurate under conditions of non-homogeneous deformation, it is assumed that the current simulation results will not change significantly for the uniform deformation conditions of uniaxial tensile strain. The strain (ε) calculated here is the engineering strain and the mean stress (σ_m) is calculated as

$$\sigma_m = (\sigma_x + \sigma_y + \sigma_z)/3 \tag{2}$$

where σ_x, σ_y, and σ_z are the stresses averaged over the entire system in the X, Y, and Z directions, respectively. An effective von Mises stress (σ_e) and an effective von Mises strain (ε_e) is calculated as

$$\sigma_e = \left[\frac{1}{2}\left((\sigma_x - \sigma_y)^2 + (\sigma_y - \sigma_z)^2 + (\sigma_z - \sigma_x)^2 + 6(\sigma_{xy}^2 + \sigma_{yz}^2 + \sigma_{xz}^2)\right)\right]^{1/2} \tag{3}$$

$$\varepsilon_e = \frac{\sqrt{2}}{3}\left[\left((\varepsilon_1-\varepsilon_2)^2+(\varepsilon_2-\varepsilon_3)^2+(\varepsilon_3-\varepsilon_1)^2\right)\right]^{1/2} \quad (4)$$

To study the effect of microstructure, nanocrystalline Cu systems were created an average grain size of 6 nm, 8 nm, 10 nm and 12 nm using the Voronoi construction method [Derlet and Van Swygenhoven 2003] with periodic boundary conditions in all the three directions. The nanocrystalline system created was cubic with sizes of 4*d* x 4*d* x 4*d* (*d* = grain size) resulting in 122 grains for all the grain sizes considered. The as-created system was first relaxed to have zero pressure, and then equilibrated at 300 K for 100 ps. The centrosymmetry parameter (CSP) [Kelchner, Plimpton, and Hamilton 1998] and the common neighbor analysis (CNA) [Honneycutt and Andersen 1987] were used to characterize the defects in the nanocrystalline system. In addition, a grain identity number (G_{id}) is assigned to each atom that defines the grain to which it belongs in the nanocrystalline system. The identity of the grain for each atom allows the monitoring of the evolution of the void surfaces during failure. The initial nanocrystalline system containing 122 grains with an average grain size of 6 nm and 12 nm is shown in Fig. 1 (a) and (b), respectively, with the atoms colored according to the CNA values. The contour for the atoms colored according to their CNA values is as follows: the yellow colored atoms represent bulk fcc stacking, the red colored atoms represent local hexagonal close-packed order (partial dislocations), the green colored atoms represent a coordination greater than 12, the light blue colored atoms represent a coordination of 12 other than fcc stacking, and the blue colored atoms represent a coordination of less than 12.

Deformation under conditions of uniaxial expansion ($\varepsilon_x = \varepsilon_y = 0$, and $\varepsilon_z = \varepsilon$) was achieved at each time step by adjusting the z coordinate of all of the atoms using a scaling parameter. The cell dimensions in the loading directions were adjusted accordingly at each step. The coordinates of the atoms and the cell dimensions in the X and Y directions were not scaled, thus resulting in zero strains in the X and Y directions. The scaling parameter was a constant chosen based on the time step and the initial system size to achieve the desired constant strain rate ($\dot{\varepsilon}$). The time step for all of the MD simulation runs was chosen to be 2 fs and the temperature was allowed to evolve during the deformation process. The effects of grain size and strain rates on the failure behavior of the nanocrystalline metal are discussed below.

3 Dynamic Failure of Nanocrystalline Cu: Grain Size Effect

Large scale MD simulations of uniaxial expansion ($\varepsilon_x = \varepsilon_y = 0$, and $\varepsilon_z = \varepsilon$) are carried out for nanocrystalline Cu with an average grain size of 6 nm, 8 nm, 10 nm, and 12 nm to investigate the effect of grain size in the inverse Hall-Petch regime at a constant strain of 10^9 s^{-1}. The evolution of the von Mises stress (σ_e) and

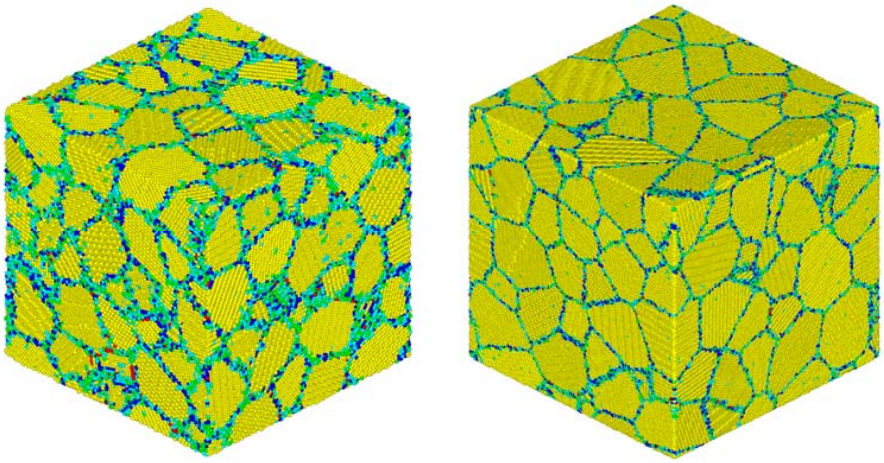

(a) (b)

Figure 1: The initial configuration of nanocrystalline Cu with 122 grains and an average grain size of (a) 6 nm, and (b) 12 nm. The atoms are colored according to the CNA values.

mean stress (σ_m) is monitored during the simulations and plotted as a function of effective von Mises strain (ε_e) in Fig. 2(a) and Fig. 2(b), respectively. The von-Mises effective stress curves are initially linear and lie on top of each other and start to deviate at the onset of GB sliding/rotation. The deviation is larger for grain sizes of 6 nm and 8 nm due to higher accommodation of stresses by GB sliding/ rotation at lower grain sizes as compared to larger grains [Vo et al. 2008Dongare et al. 2010b]. The effective stress increases to a peak value after which it drops due to accommodation of strain by the nucleation of dislocations from the grain boundaries. The drop in effective stresses is observed to increase with grain sizes due to increased dislocation activity at the larger grain sizes [Dongare et al. 2010]. The drop in effective stresses continues till the mean stress reaches a peak value after which a concurrent sharp drop in the effective and mean stresses is observed to reach a minimum value. This drop is attributed to the nucleation of voids at grain boundaries. Previous MD simulations [Dongare et al. 2009b] demonstrate two stages of void growth under conditions of uniaxial tensile strain for nanocrystalline Cu with an average grain size of 6 nm at a constant strain of 10^8 s^{-1}. The time duration of the drop of the mean stresses to a minimum value corresponds to the time duration of the first stage (I) of void growth. The peak value of the mean stress

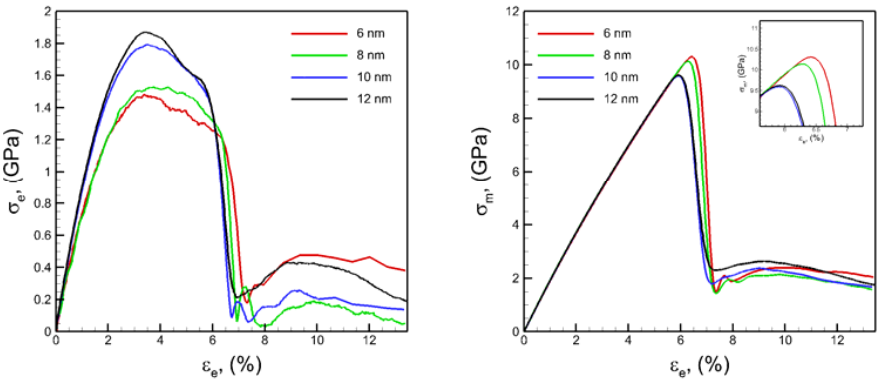

(a) (b)

Figure 2: Plots of (a) effective von Mises stress (σe), and (b) mean stress (σm), as a function of effective von Mises strain (εe) during tensile deformation under uniaxial strain of a nanocrystalline copper sample with an average grain size of 6 nm (red curve), 8 nm (green curve), 10 nm (blue curve), and 12 nm (black curve) at a constant strain rate ($\dot{\varepsilon}$) of 10^9 s^{-1}.

can be related to the spall strength of the metal. The MD simulations show that the nanocrystalline metal with an average grain size of 6 nm has the highest value for the spall strength for a constant strain of 10^9 s^{-1}. These values compare well with the spall pressures predicted during spallation experiments [Moshe et al. 1998]. The spall strength of the metal and the strain at which the metal begins to fail by nucleation of voids is observed to decrease with an increase in grain size up 10 nm after which a slight increase is observed at an average grain size of 12 nm for a constant strain rate of 10^9 s^{-1}. The relaxation of stresses to reach a minimum as shown in Fig. 2 corresponds to the onset of the second stage (II) of void growth, during which, evolution of voids occurs at a steady rate. An intermediate snapshot of the nanocrystalline system is illustrated in Fig. 3(a) and (b) for a grain size of 6 nm and 12 nm, respectively at the time/strain corresponding to the minimum in the mean stress values. The distribution of voids in the nanocrystalline system is illustrated in Fig. 3(c) and (d) for the grain size of 6 nm and 12 nm, respectively. A larger number of voids and larger number of dislocations are observed for the system with a grain size of 12 nm as compared to that with the 6 nm grain size.

In addition, to have a quantitative understanding of the effect of grain size on the void growth behavior, the evolution of the void fraction (V_f) and the number of voids (N_V) is monitored during the simulation. The porosity or void fraction (V_f),

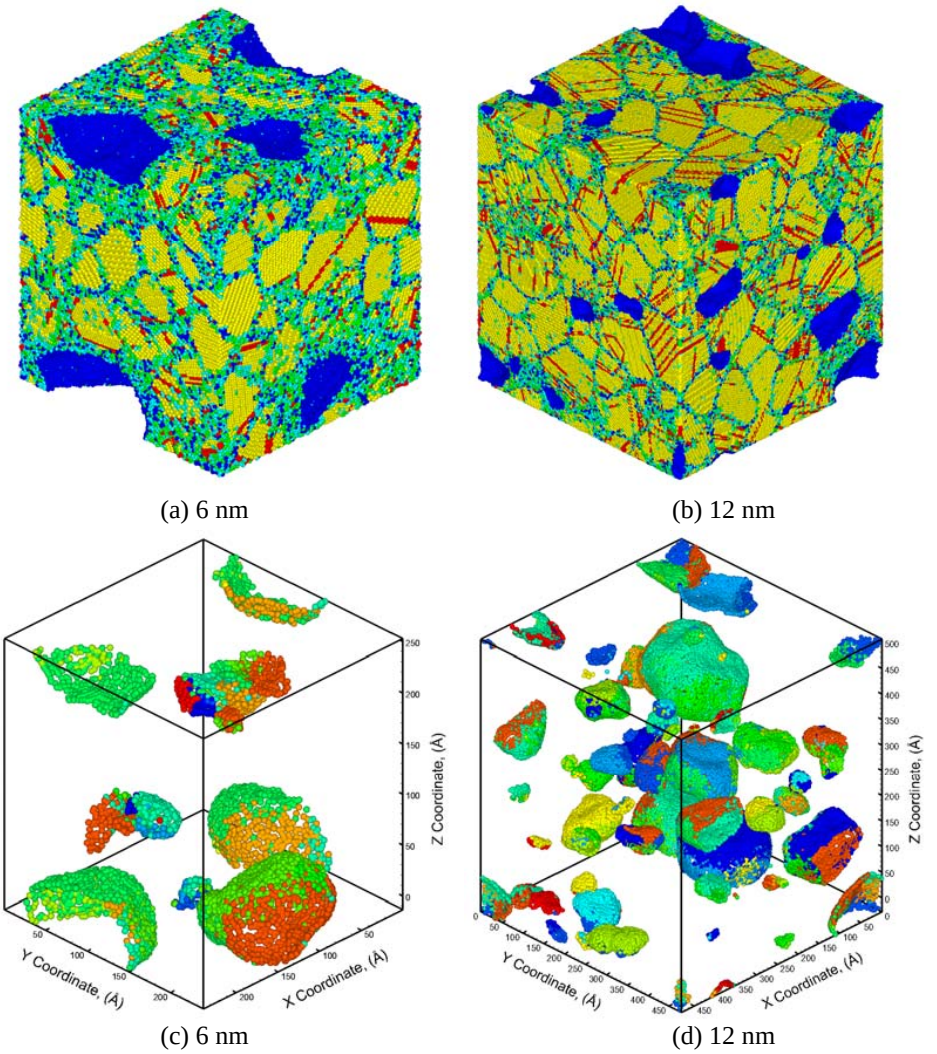

(a) 6 nm (b) 12 nm

(c) 6 nm (d) 12 nm

Figure 3: (a) Snapshot the nanocrystalline Cu sample with an average grain size of (a) 6 nm and (b) 12 nm, with atoms colored according to the CNA values at the critical effective strain during uniaxial expansion a constant strain rate of $10^9 s^{-1}$. The void distribution in the nanocrystalline metal is shown in (c) for an average grain size of 6 nm and in (d) for an average grain size of 12 nm. The atoms in (c) and (d) are colored according to the grain id (Gid) number.

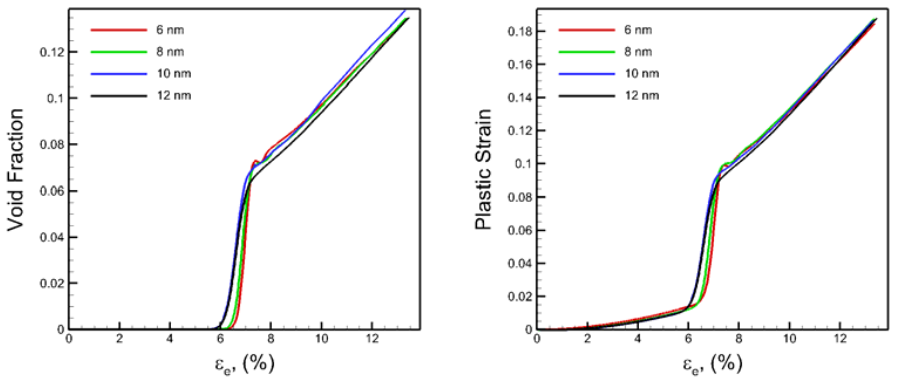

(a) (b)

Figure 4: Plots of (a) void fraction (Vf), and (b) plastic strain as a function of effective strain for various grain sizes during uniaxial expansion of nanocrystalline Cu with an average grain size of 6 nm at a strain rate ($\dot{\varepsilon}$) of 10^9 /s.

defined as the ratio of the total volume of the voids (V_v) to the total volume (V_{tot}) of the system ($V_f = V_v/V_{tot}$), is calculated during the course of the simulations. To calculate the void fraction, a three-dimensional grid of cubic cells is superimposed over the atomic configuration, and clusters of two or more contiguous empty cells are identified as voids [Zhigilei et al. 2004; Dongare et al. 2009b]. The total volume of the empty cells divided by the volume of the cells is calculated as the void fraction. The cell size (0.36 nm) is chosen so as to have at least several atoms in the cell for the case without any voids.

The plastic strain (ε_p) is calculated using the general form of the Hooke's law:

$$\sigma_{ij} = \lambda e_{kk}\delta_{ij} + 2\mu e_{ij} \tag{5}$$

The evolution of the void fraction and plastic strain as a function of effective strain is shown in Fig. 4(a) and (b), respectively. The plots show two stages of void growth that coincide with the two stages for the evolution of the plastic strain [Dongare et al. 2009b]. The first stage (I) corresponds to the nucleation of voids and the fast linear growth of all the individual voids. The onset of the second stage (II) of void growth corresponds to the steady growth (slightly slower) of the void aggregates that eventually form the fracture surface. The initial plastic strain at which the void fraction is zero is attributed to GB sliding and dislocation induced plasticity and hence the curves are on top of each other prior to void nucleation. Nucleation of voids causes the curves to deviate from each other during stage I of void growth

and then fall again on top of each other as the effective strain corresponding to the onset of stage II of void growth. The evolution of the void fraction as a function of effective strain during stage II is observed to be independent of the grain size of the metal. The initial plastic strain at which the void fraction is zero is attributed to GB sliding, after which the evolution of the plastic strain is observed to be consistent with the evolution of the void fraction during stage I and stage II of void growth. The evolution of number of voids as a function of plastic strain is shown in Fig. 5. The plots show an increased number of voids nucleated (and therefore a faster nucleation rate) for the system with a grain size of 12 nm as compared to that for 6 nm grain size. The time duration of the nucleation of voids, however, is observed to the independent of the grain size of the nanocrystalline metal. The effects of strain rates on the failure behavior of the nanocrystalline metal are discussed below.

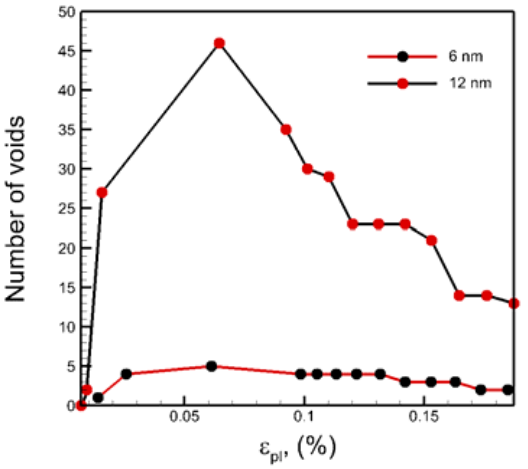

Figure 5: Plot of number of voids as a function of plastic strain during uniaxial expansion of nanocrystalline Cu with an average grain size of an average grain size of 6 nm and 12 nm f 6 nm at a strain rate ($\dot{\varepsilon}$) of 10^9 /s.

4 Effect of Strain Rate on Dynamic Failure Response of Nanocrystalline Cu

The effect of strain rate on the failure behavior is demonstrated for a 6 nm grain size nanocrystalline Cu sample MD simulations of uniaxial expansion of are carried out at strain rates ranging from $4x10^7 s^{-1}$ to 10^{10} s^{-1}. The plots of the mean stress and the von Mises stress as a function of effective strain are shown below in Fig. 6 (a) and (b), respectively. The plots show that the strain rate has a strong effect on

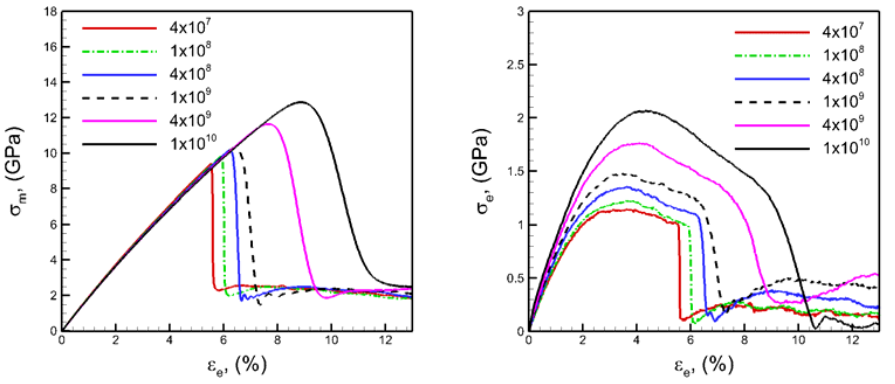

(a) (b)

Figure 6: Plots of (a) von Mises stress, and (b) mean stress, as a function of effective strain during tensile deformation under uniaxial strain of a nanocrystalline Cu with an average grain size of 6 nm. The strain rates ($\dot{\varepsilon}$) used vary from 4x107 s^{-1} to 1010 s^{-1}.

the stress-strain curves during deformation. The mean stress curves lie on top of each other during elastic expansion and then start to deviate due to nucleation of voids. The von Mises curves, on the other hand do not lie on top of each other. The deviation is observed to increase at higher strain rates. The curves show higher peak von Mises stress values as the strain rate increases that suggests limited relaxation due to GB sliding at higher strain rates [Bringa et al. 2005]. The relaxation of effective stresses due to nucleation of dislocations is also observed to be larger at higher strain rates. The peak value of the spall strength of the nanocrystalline metal is observed to increase with the loading strain rates. The spall strengths computed here compare very well with those predicted experimentally [Moshe et al. 1998].

The void fraction and plastic strain are plotted as a function of time in Fig. 7(a) and (b), respectively as a function of effective strain for the various strain rates. It can be seen from the plots that the transition from a fast initial growth of individual voids to a more steady growth of void aggregates becomes slower as the strain rate increases. This slower transition at higher strain rates is due to the larger strains required for the nucleation of larger number of voids at higher strain rates of deformation. An intermediate snapshot of the nanocrystalline system is illustrated in Fig. 8(a) at an effective strain corresponding to the critical void fraction at a constant strain rate of 10^{10} s^{-1}. The contour for the atoms colored according to their CNA values is the same as in Fig. 1. The distribution of voids in the nanocrystalline

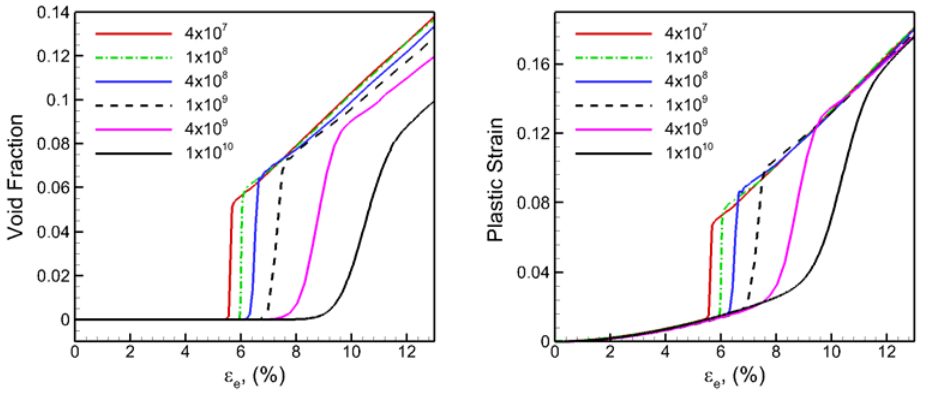

Figure 7: Plots of evolution of (a) void fraction, and (b) plastic strain as a function of effective strain during tensile deformation under uniaxial strain of a nanocrystalline Cu with an average grain size of 6 nm. The strain rates ($\dot{\varepsilon}$) used vary from $4\text{x}10^7$ s^{-1} to 10^{10} s^{-1}.

system is illustrated in Fig. 8(b). The void is obtained by showing only the atoms having a CSP value corresponding to a surface. A comparison of these snapshots with those in Fig. 3(a) and (c) shows a larger number of voids that are smaller in size at a strain rate of 10^9 s^{-1}.

The evolution of the plastic strain during Stage I is observed to be strongly dependent of the strain rate of deformation. The plastic strain corresponding to nucleation of voids and the onset of Stage II is observed to increase with increasing strain rates. However, a striking behavior in the evolution of plastic strain and the evolution of void fraction is that the curves fall back on top of each other during stage II of void growth even at a strain rate of 10^{10} s^{-1}. This suggests that the evolution of plastic strain during stage II is independent of the strain rate of deformation, whereas the evolution of void fraction during stage II is strongly dependent on the strain rate of deformation. To quantify the effects of strain rate of deformation on void growth, the effective strain (ε_e^n) associated with the nucleation of voids, the *critical* void fraction (V_f^c), and the *critical* effective strain (ε_e^c) corresponding to the onset of stage II growth, are identified as a function of strain rate ranging from $4\text{x}10^7$ s^{-1} to 10^{10} s^{-1} and tabulated above in Table 1.

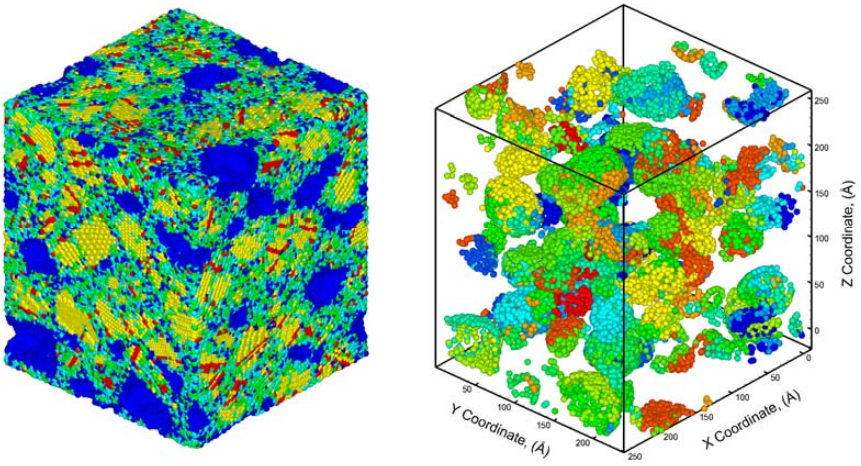

(a) Δ_{csp} (b) G_{id}

Figure 8: (a) Snapshot the nanocrystalline Cu sample with an average grain size of 6 nm with the atoms colored according to the CNA values at the critical effective strain during uniaxial expansion a constant strain rate of 10^{10} s^{-1}. The void distribution in the nanocrystalline metal is shown in (b) with the atoms colored according to the grain id (Gid) number.

Table 1: Void fractions, the effective strains and the plastic strains as obtained from MD simulations at strain rates from 4 x 10^7 s^{-1} to 1 x 10^{10} s^{-1}. V_f^c is the critical void fraction attributed to the onset of stage II of void growth. Similarly, ε_e^n corresponds to the effective strain associated with the nucleation of voids and ε_e^ccorresponds to the critical effective strain corresponding to the onset of stage II growth.

	4 x 10^7 s^{-1}	10^8 s^{-1}	4 x 10^8 s^{-1}	10^9 s^{-1}	4 x 10^9 s^{-1}	10^{10} s^{-1}
$\varepsilon_e^n(\%)$	5.55	5.93	6.23	6.43	7.64	8.88
$\varepsilon_e^c(\%)$	5.78	6.21	6.64	7.33	9.90	13.30
$V_f^c(\%)$	5.37	6.00	6.40	7.25	8.94	10.26

5 Relevance to Continuum Modeling of Spallation

Molecular Most of the modeling of void growth and porosity has been carried out using continuum models [Gurson 1977; Needleman 1972; Tvergaard 1990; Tvergaard and Needleman 1984]. The yielding of the metal at the continuum scale in

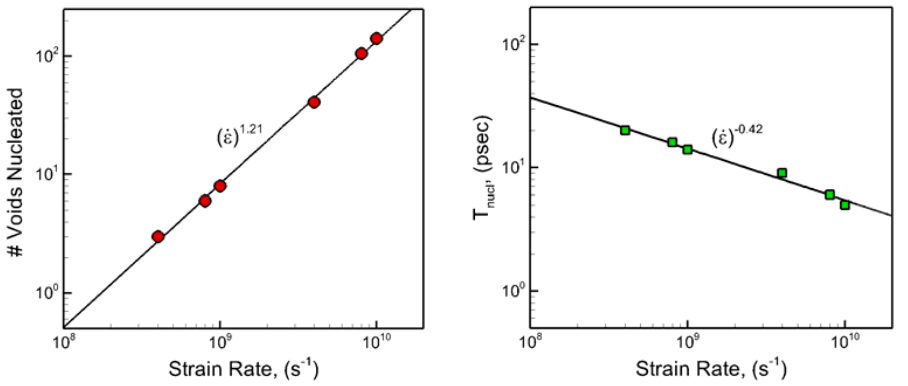

(a) (b)

Figure 9: Power-law plots of (a) number of voids nucleated (N_V), and (b) the time duration of stage I i.e. nucleation of voids (T_{nucl}), as a function of strain rate ($\dot{\varepsilon}$) ranging from 4x10^8 s^{-1} to 10^{10} s^{-1}.

these models is defined by equation (7).

$$\phi = \left(\frac{\sigma_e}{\sigma_{YS}}\right)^2 + 2q_1 V_f \cosh\left\{\frac{3q_2\sigma_m}{2\sigma_{YS}}\right\} - \left[1 + q_3(V_f)^2\right] = 0, \tag{6}$$

for $V_f \leq V_f^c$.

where, σ_e, and σ_m, are the von Mises stress and mean stress of the void containing aggregate, respectively. The parameters (q_1, q_2, q_3) are parameters used to fit the experimental data. The void fraction (porosity), V_f, is defined as the ratio of the total void volume to that of the system, and V_f^c is the critical void fraction for coalescence. These models assume that the voids are spherical or cylindrical and that the dilation of the void-matrix aggregate is completely due to void growth. In addition, it should be noted that the evolution of porosity in these models is determined by a single parameter, the void fraction, which is independent of the microstructure and strain rate. The MD simulations of dynamic failure reported here validate the assumption that the voids are spherical at the onset of dynamic failure.

At the continuum level, the change in the void fraction (ΔV_f) at any instance of time can be given as the sum of the changes in the void fractions due to nucleation of new voids ($\Delta V_{nucleation}$) and due to the growth of existing voids (ΔV_{growth}) [Tvergaard and Needleman 1984]. The nucleation of voids is controlled by plastic strain, and the coalescence process occurs above a certain critical value for the void frac-

tion. The MD simulations discussed here quantify these strains and void fractions and suggest that after the initial nucleation of voids during stage I, the change in void fraction is attributed to the growth and coalescence of the existing individual voids only. Nucleation of new voids is not observed once the critical void fraction is reached. The critical void fraction is found to increase with an increase in strain rate of deformation, but, it is less sensitive to the average grain size of the system. As a result, the void growth behavior can be characterized as the sum of the change in void fraction due to growth and coalescence of individual voids during stage I (ΔV_f^I), and the change in void fraction due to the growth of the void aggregate (ΔV_f^{II}). The dependencies of the two stages of growth as observed using MD simulations can be used to design evolution laws for continuum simulations.

6 Conclusions

Molecular dynamics simulations are carried out to understand the effects of grain size and loading strain rates on the nucleation, growth, and coalescence of nanoscopic voids under conditions of deformation that lead to the onset of spallation of metals during shock loading. The spall strength of the nanocrystalline metal is observed to be strongly dependent on the strain rate and less dependent on the grain size in the inverse Hall-Petch regime. The spall strength is observed to increase with increasing strain rate and results in delayed failure of the nanocrystalline metal. The evolution of voids is observed to be strongly dependent on the strain rates with larger number of voids nucleated in shorter amounts of times at higher strain rates. For the same number of grains in the system, a larger number of voids are observed for larger grain sizes. Since the void fraction is less affected by the grain size, the average size of the void is smaller at larger grain sizes. The void fraction, however, is observed to be strongly affected by the strain rate. For a given value of effective strain, the void fraction of the system is smaller at higher strain rates. A power-law dependence on the loading strain rates is observed for the number of voids nucleated and the time duration for nucleation of voids for the nanocrystalline sample. This power-law dependence reflects the general characteristics of the failure behavior of nanocrystalline Cu at high strain rates.

Acknowledgement: The research was supported by the U. S. Army Research Office (ARO) through the National Research Council Research Associateship Program.

References

Bringa, E. M.; Caro, A.; Wang, Y.; Victoria, M.; McNaney, J. M.; Remington, B. A.; Smith, R. F. ; Torralva, B. R.; Van Swygenhoven, H. (2005): Ultrahigh strength in nanocrystalline materials under shock loading. Science, vol. 309, pp. 1838-1841.

Curran, D.R.; Seaman, L.; Shockey, D.A. (1987): Dynamic failure of solids. *Phys. Rep.,* vol. 147, pp. 253-388.

Derlet P. M.; Van Swygenhoven, H. (2003): Atomic positional disorder in fcc metal nanocrystalline grain boundaries. Phys. Rev. B, vol. **67**, pp. 014202.

Dongare, A. M.; Rajendran, A. M.; LaMattina, B.; Zikry, M. A.; Brenner, D. W. (2008) Atomic scale simulations of orientation of loading axis on the growth of voids at the onset of ductile failure in single crystal Cu. *Mat. Res. Soc. Sym. Proc.*, vol. 1137, pp. EE08-09-W10-09.R1.

Dongare, A. M.; Rajendran, A. M.; LaMattina, B.; Zikry, M. A.; Brenner, D. W. (2009a): Atomistic studies of void-growth based spall failure in single crystal copper at high strain rates, Shock Compression of Condensed Matter - 2009, AIP Conference Proceedings. vol. 1195, pp. 769-772

Dongare, A. M.; Rajendran, A. M.; LaMattina, B.; Zikry, M. A.; Brenner, D. W. (2009b): Atomic scale simulations of ductile failure micromechanisms in nanocrystalline Cu at high strain rates, *Phys. Rev. B*, vol. 80, pp. 104108.

Dongare, A. M.; Rajendran, A. M.; LaMattina, B.; Zikry, M. A.; Brenner, D. W. (2010a): Atomic scale studies of spall behavior in nanocrystalline Cu, J. Appl. Phys. Vol. 108, pp. 113518.

Dongare, A. M.; Rajendran, A. M.; LaMattina, B.; Zikry, M. A.; Brenner, D. W. (2010b): Atomic scale study of plastic-yield criterion in nanocrystalline metals using molecular dynamics simulations. *Metall. Mater. Trans. A*, vol. 41A, pp. 523-531.

Eliezer, S.; Gilath, I.; and Bar-Noy, T. (1990): Laser-induced spall in metals: Experiment and simulation. *J. Appl. Phys.*, vol. 67, pp. 715.

Fowler, J. P.; Worswick, M. J.; Pilkey, A. K.; Nahme H. (2000): Damage leading to ductile fracture under high strain-rate conditions. *Metall. Mater. Trans. A* ,vol. 31, pp. 831-844.

Gurson, A. L. (1977): Continuum theory of ductile rupture by void nucleation and growth: Part 1 – Yield Criteria and Flow rules for porous ductile. *J. Eng. Mater. Technol.*, Vol. **99**, pp. 2-15.

Honneycutt, D. J.; Andersen, H. C. (1987): Molecular dynamics study of melting and freezing of small Lennard-Jones clusters. *J. Phys. Chem.*, vol. 91, pp. 4950-

4963.

Kanel, G. I.; Razorenov, S. V.; Utkin, A. V.; Fortov, V. E.; Baumung, K.; Karow, H. U.; Rusch, D.; and Licht, V. (1993): Spall strength of molybdenum single crystals, *J. Appl. Phys.*, vol. 74, pp. 7162.

Kelchner, C. L.; Plimpton, S. J.; Hamilton, J. C. (1998): Dislocation nucleation and defect structure during surface indentation. *Phys. Rev. B*, vol. 58, pp. 11085-11088

Knott, J. F. (1973): *Fundamentals of Fracture Mechanics*, Butterworths, London.

Leveugle E.; Zhigilei, L. V. (2004): Microscopic mechanisms of short pulse laser spallation of molecular solids. *Appl. Phys. A*, vol. 79, pp. 753-756.

Meyers, M. A. (1994): *Dynamic Behavior of Materials* (Wiley-Interscience, New York, 1994)

Minich, R. W.; Cazamias, J. U.; Kumar, M.; and Schwartz, A. J. J. (2004): Effect of microstructural length scales on spall behavior of copper. *Metall. Mater. Trans. A*, vol. 35, pp. 2663-2673.

Moshe, E.; Eliezer, S.; Dekel, E.; Ludmirsky, A.; Henis, Z.; Werdiger, M.; Goldberg, I. B.; Eliaz, N.; and Eliezer, D. (1998):An increase of the spall strength in aluminum, copper, and Metglas at strain rates larger than 10^7 s^{-1}, *J. Appl. Phys.*, vol. 83, pp. 4004.

Moshe, E.; Eliezer, S.; Dekel, E.; Henis, Z.; Ludmirsky, A.; Goldberg, I. B.; and Eliezer, D. (1999): Measurements of laser driven spallation in tin and zinc using an optical recording velocity interferometer system. *J. Appl. Phys*., vol. 86, pp. 4242.

Needleman A.; (1972): Void growth in an elastic plastic medium. J. Appl. Mech., vol. 39, pp. 964-970.

Rajendran, A. M.; Dietenberger, M. A.; Grove, D. J. (1989): A void growth-based failure model to describe spallation. *J. Appl. Phys.*, vol. **65**, pp. 1521.

Rivas, J. M.; Zurek, A. K.; Thissell, W. R.; Tonks, D. L.; Hixson, R. S. (2000): Quantitative description of damage evolution in ductile fracture of tantalum. *Metall. Mater. Trans. A*, vol. 31, pp. 845-851.

Seppala, E. T., Belak J., and Rudd, R.E. (2004): Effect of stress triaxiality on void growth in dynamic fracture of metals: A molecular dynamics study. *Phys. Rev. B*, vol. 69, pp. 134101.

Seppala, E. T.; Belak J.; and Rudd, R.E.; (2004): Onset of void coalescence during dynamic fracture of ductile metals. *Phys. Rev. Lett*., Vol. 93, pp. 245503.

Seppala, E. T.; Belak, J.; Rudd, R.E. (2005): Three-dimensional molecular dy-

namics simulations of void coalescence during dynamic fracture of ductile metals. *Phys. Rev. B*, vol. 71, pp. 064112.

Shen, S. P. and Atluri, S. N. (2004): Atomic-level Stress Calculation and Continuum-Molecular System Equivalence, *CMES: Computer Modeling in Engineering & Sciences*, Vol. 6, No. 1, pp. 91-104.

Strachan, A.; Ça?ın, T.; Goddard, III, W. A. (2001): Critical behavior in spallation failure of metals. Phys. Rev. B, vol. 63, pp. 060103.

Tamura, H.; Kohama, T.; Kondo, K.; Yoshida, M. (2001): Femtosecond-laser-induced spallation in aluminum, *J. Appl. Phys.,* vol. 89, pp. 3520-3522.

Thomason, P. F. (1999): Ductile spallation fracture and the mechanics of void growth and coalescence under shock-loading conditions. Acta Mater., vol. 47, pp. 3633-3646.

Traiviratana, S.; Bringa, E. M.; Bensona, D. J.; Meyers, M. A. (2008): Void growth in metals: Atomistic calculations. *Acta Mater.*, vol. 56, pp. 3874-3886 .

Tvergaard, V.; Needleman, A. (1984): Analysis of the cup-cone fracture in a round tensile bar. *Acta Metall.*, vol. 32, pp. 157-169.

Tvergaard, V.; (1990): Material failure by void growth to coalescence. *Adv. Appl. Mech*., vol. 27, pp. 83-151.

Vo, N. Q.; Averback, R. S.; Bellon, P.; Odunuga, S.; Caro, A. (2008): Quantitative description of plastic deformation in nanocrystalline Cu: Dislocation glide versus grain boundary sliding. *Phys. Rev. B*, vol. 77, pp. 134108.

Voter, A. F. (1994): The Embedded Atom Method. In: *Intermetallic Compounds: Principles and Practice*. Edited by J. H. Westbrook and R. L. Fleischer, Wiley, New York, pp. 77.

Wright, T. W.; and Ramesh, K. T. (2008): Dynamic void nucleation and growth in solids: A self consistent statistical theory. *J. Mech. Phys. Solids*, vol. **56**, pp. 336 -359.